PHYSICAL REVIEW B **112**, 045305 (2025)

Bipolarons on dry and wet reduced rutile (110) surfaces: A constrained density functional theory study

Yun-Bo Li,[1,2] Da-Wei Deng,[1,2] Wen-Jin Yin,[1,2,3,*] Nicola Seriani,[3] and Ralph Gebauer[3,†]
[1] *School of Physics and Electronic Science, Hunan University of Science and Technology, Xiangtan 411201, China*
[2] *Key Laboratory of Intelligent Sensors and Advanced Sensing Materials of Hunan Province, Hunan University of Science and Technology, Xiangtan 411201, China*
[3] *The Abdus Salam International Centre for Theoretical Physics (ICTP), Strada Costiera 11, I-34151 Trieste, Italy*

(Received 21 January 2025; revised 29 May 2025; accepted 20 June 2025; published 7 July 2025)

Defects have a profound effect on the electronic and transport behavior of materials. They play an important role in many photoelectric devices. Here, we investigate by means of constrained density functional theory (C-DFT) the spatial distribution and transport properties of bipolarons that are induced by surface oxygen vacancies (O_v) on reduced rutile TiO_2 (110) surfaces. We find that bipolarons preferentially localize in a subsurface geometry, followed by a mixed surface-subsurface localization, while a surface state is the energetically least preferred location for bipolarons. We show that this unique behavior is caused by an interplay of the splitting of titanium d orbitals, the orbital symmetry, and the electrostatic potential. Also, the polaron transport properties are examined, both parallel and perpendicular to the surface. The introduction of water molecules on the surface can effectively lead to the transfer of subsurface polarons to a position on the surface. The preferred transfer direction of polarons changes from the [001] direction to the [110] direction when the water coverage exceeds one-half monolayer. This characteristic behavior is strongly related to the synergetic effect of the electronic coupling strength and the transition barrier at different water coverages. Our findings reveal the energetic order of bipolaron localizations, their transport properties, and the effect of water on a reduced rutile TiO_2 (110) surface, hence leading to a better understanding of the role of polarons in photoelectric applications.

DOI: 10.1103/ckws-yk2c

I. INTRODUCTION

Rutile TiO_2, a prototypical transition metal oxide, has garnered significant interest in photocatalysis and electrocatalysis due to its unique optoelectronic properties [1,2]. However, its practical utility remains constrained by two intrinsic limitations, a wide band gap that limits light absorption to the ultraviolet regime and a low carrier transport that prohibits the enhancing of photoelectric efficiency [3–5]. To overcome these challenges, defect engineering has emerged as a transformative strategy for tailoring the electronic landscape of TiO_2. For instance, Cheng *et al.* [6] precisely manipulated the electronic structure by introducing Ti^{3+} into the porous single-crystalline rutile lattice, which can effectively enhance the photocatalytic performance and achieve a maximal photoelectric current response. Additionally, Wu *et al.* [7] fabricated photoelectric diodes utilizing Ti^{3+} self-doped TiO_2 nanoparticles, exhibiting strong light absorption and efficient charge carrier transport capability. Furthermore, Liang *et al.* [8] designed a unique P^{3+}-O_v-Ti^{3+} doping structure within TiO_{2-x} nanotube arrays, allowing for a modulation of the electronic structure and the establishment of electron transfer pathways. During this process, strong interactions occur between the photogenerated carriers and Ti atoms of the TiO_2 lattice, leading to the formation of a stable polaron state that persists throughout the charge transport process. This polaron state significantly prolongs the carrier lifetime, thereby contributing to improved photoelectric conversion efficiency. Consequently, investigations associated with the polaron state within TiO_2 are of great importance.

Despite critical insights, the atomistic behavior of polarons in rutile TiO_2 remains contentious. In rutile TiO_2, excess electrons tend to couple with Ti^{4+} ions, forming a reduced state of Ti^{3+} ions. It has been predicted that Ti^{3+} accompanied with lattice distortions in the surrounding environment collectively forms a small polaron. From the experimental side, authors of several studies have focused on the polaronic states at the surface of oxygen vacancy-defective rutile TiO_2 (110) [2,9]. Including also the theoretical side, Shibuya *et al.* [10,11] systematically investigated the polaron models at the O_v defective rutile TiO_2 (110) surface from both theoretical [density functional theory-based HSE06 (DFT+HSE06)] and experimental [scanning tunneling microscopy (STM)] perspectives. They found that the two excess electrons tend to occupy the Ti sites at different rows of the subsurface layers. This conclusion is highly analogous to the predictive results obtained by Deskins *et al.* [12] with the DFT+U method. Unlike above, Di Valentin *et al.* [13] suggested that the two excess electrons of oxygen vacancies tend to occupy the two fivefold-coordinated Ti positions at the surface according to a hybrid B3LYP calculation. Further DFT+U calculations proposed by Calzado *et al.* [14] demonstrated that the spatial distribution was related to O_v

---

[*] Contact author: ywj@hnust.edu.cn

[†] Contact author: rgebauer@ictp.it

concentration. Except for the above methods, it has been reported that the piecewise linear functional including PBE0(α), γDFT, and DFT+U is also an efficient method to model the polaron in transition metal oxides [15,16]. Excess electrons are often found in the interior at low defect concentration, while they are observed to occupy surface positions in the high concentration case. The surface bipolarons on reduced rutile TiO_2 (110) surfaces cannot remain stable at one fixed position since its location is influenced by factors such as the mobility of excess electrons and the concentration of oxygen vacancies. Therefore, it is crucial to investigate the formation mechanism, the electronic structure, and their impact on the photocatalytic performance of bipolarons in detail.

Apart from the polaron distribution, the migration of small polarons in rutile TiO_2 directly impacts the photocatalytic efficiency of semiconductor structures. Authors of studies have revealed a pronounced anisotropy in the migration of polarons along different directions. Through two-photon photoemission spectroscopy, Li *et al.* [17] have shown the characteristic $3d \rightarrow 3d$ transitions of Ti^{3+} ions in rutile TiO_2, a finding that is consistent with findings by Wang *et al.* [18]. Authors of further investigations have identified the anisotropic nature of these $3d \rightarrow 3d$ transitions, which can be selectively excited and conducted by the polarization of light. Additionally, Yan *et al.* [19] reported that the activation energies for polaron migration along the [001] and [111] directions are separately 0.026 and 0.195 eV, respectively, showing a preference for transfer along the [001] direction, which is a result similar to that of Janotti *et al.* [20]. Using semiclassical Marcus theory, Morita *et al.* [21] analyzed the transport mechanisms of polarons in different crystal environments, and they proposed a computational method for the polaron transport. Despite the vast number of proposed mechanisms to understand polaron transport in rutile TiO_2, several challenges persist in this area of research, like for example, a better understanding of the role of O_v defects in charge transport.

Especially in real applications, it is inevitable to encounter a wet environment. Thus, understanding the interplay between polarons and water molecules is fundamental for numerous photocatalytic applications. Using first-principles nonadiabatic molecular dynamics (NAMD) calculations, Fischer *et al.* [22] investigated the electron polaron transfer at TiO_2 surfaces, and they found that a close electronic coupling between water molecules and TiO_2 facilitates a rapid electron transfer to the surface. Similarly, Gao *et al.* [23] also employed NAMD techniques to study the capture process of photoexcited electrons at rutile TiO_2 (110) surfaces. Their discoveries indicate that water molecules can elongate the surrounding Ti-O bond lengths, stabilizing surface polaron and shortening the lifetime of photoexcited polarons, thereby enhancing photocatalytic activity. Recently, employing a constrained DFT approach, Li *et al.* [24] systematically studied the local and transport effects of water molecules on surface polarons on rutile TiO_2 (110). Under dry conditions, excess electrons tend to form localized small polarons at subsurface Ti sites, with superior transport properties along the [001] direction. However, under water coverage, small polarons can be extracted to surface Ti sites saturated with water molecules. Even the transport mode can be changed from the [001] direction to the [110] direction when the water coverage is larger than one-half monolayer. Despite these important findings, systematic studies of the spatial distribution of defect-induced polarons and of their transport in wet conditions are still needed for a more detailed understanding. In this work, we aim at understanding the spatial distribution and the transport behavior as well as the role of water on polarons induced by O_v on reduced rutile TiO_2 (110) surfaces by constrained DFT (C-DFT). First, the localization and spatial distribution of polarons induced by surface O_v will be discussed as well as their key transport behavior. Next, the water effects on the stability and transport properties of bipolarons are further studied. Finally, the underlying mechanism of the polaron localization and transport will be discussed considering the orbital splitting and symmetry.

II. COMPUTATIONAL METHODS

All calculations were carried out by C-DFT as implemented in the CP2K/QUICKSTEP package [25], which is based on a hybrid Gaussian and plane-wave basis set. The exchange-correlation energy was approximated by the Perdew-Burke-Ernzerhof (PBE) form of the generalized gradient approximation (GGA) [26]. Goedecker-Teter-Hutter pseudopotentials were used for electron-nuclear interactions. A double-ζ plus polarization basis set was chosen for all simulations. The energy cutoff was set to 500 Ry, numerically yielding a force converged to 0.001 eV/Å. The convergence criterion for the self-consistent DFT solution was set to 10^{-6} eV between two consecutive electronic simulation steps. Different from the piecewise linear functional method including PBE0(α), γDFT, and DFT+U [15], a Hubbard-U correction (PBE+U) obtained from linear response was applied to Ti 3d orbitals with $U = 4.2$ eV [27,28]. A vacuum space of 25 Å is applied during the calculations to avoid the possible interaction between the adjacent images. A van der Waals correction based on Grimme's D3 scheme was included to account for the dispersion interaction [29].

The stability of the bipolarons is evaluated by the relative energies of the bipolarons occupied in different sites, as expressed by

$$E_{\mathrm{diff}} = E_{\mathrm{other}} - E_{\mathrm{lowest}}, \tag{1}$$

where E_{diff}, E_{other}, and E_{lowest} are the relative energy, any other cases, and the lowest total DFT energy of the bipolarons, respectively.

To understand the underlying mechanism of the spatial distribution of the bipolarons, a typical electrostatic interaction based on a point charge model is applied, which can be written as

$$W_n = \frac{1}{8\pi\varepsilon_0\varepsilon_{\mathrm{rutile}}} \sum_{j=1}^{n} \sum_{i=1}^{n} \frac{q_i q_j}{r_{ji}}, \tag{2}$$

where ε_0 is the dielectric constant in vacuum, $\varepsilon_{\mathrm{rutile}}$ is the relative dielectric constant of rutile TiO_2 [30], q_i and q_j are the charges of the polarons and of charged O_v at sites i and j ($i \neq j$), and r_{ji} represents the distance between each charged site above.

The transport behavior of a polaron is mainly determined by the transmission probability coefficient, as expressed by [31]

$$\kappa = \frac{2P_{12}^{O}}{1 + P_{12}^{O}}, \tag{3}$$

where the hopping probability P_{12}^{o} of polarons to the final site through the intersection can be obtained according to Brunschwig *et al.* [32] and Zener *et al.* [33,34], with the expression as

$$P_{12}^{O} = 1 - \exp\left[-\left(\frac{H_{\alpha\beta}^{2}}{h\upsilon_n}\right)\left(\frac{\pi^3}{\lambda k_B T}\right)^{1/2}\right], \tag{4}$$

where υ_n is a typical frequency for nuclear motion [35].

As the transmission probability coefficient κ approaches one, it represents an adiabatic transport process, and the transmission rate and hopping potential energy can be calculated as [32]

$$k_{et} = \upsilon_n \exp\left[\frac{-\Delta G_{ad}^{*}}{k_B T}\right], \tag{5}$$

$$\Delta G^{*} = \frac{\lambda}{4} - H_{\alpha\beta}. \tag{6}$$

As the transmission probability coefficient κ approaches zero, it indicates a nonadiabatic transport process. The transmission rate can be obtained according to the Marcus theory, which can be expressed as [36]

$$k_{et} = \frac{|H_{\alpha\beta}|^2}{\hbar}\sqrt{\frac{\pi}{\lambda k_B T}}\exp\left[-\frac{\Delta G^{*}}{k_B T}\right], \tag{7}$$

where $\hbar$ is the reduced Planck constant, k_B is the Boltzmann constant, λ is the reorganization energy, and T is the room temperature. Here, $H_{\alpha\beta}$ is the electronic coupling constant between the initial (Ψ_α) and final (Ψ_β) states, a little different from that obtained from the difference between bonding and antibonding energy levels [15], and it can be calculated by

$$|H_{\alpha\beta}| = |\langle\Psi_\alpha|\hat{H}|\Psi_\beta\rangle|. \tag{8}$$

Relative to some reported transition barrier obtained from the nudged elastic band method [15], the transition barrier under this condition can be calculated as [37]

$$\Delta G^{*} = -\frac{\lambda}{4} + \frac{\sqrt{\lambda^2 + 4|H_{\alpha\beta}|^2}}{2} - H_{\alpha\beta}. \tag{9}$$

It should be mentioned that, in the polaron hopping regime studied here, the electronic coupling between Ti^{3+} sites is expected to be much smaller than the nuclear reorganization energy. This places the charge transfer in the nonadiabatic (Landau-Zener) regime, where the electron tunneling probability at the crossing of diabatic potential energy surfaces is significantly less than unity. In other words, polarons on the TiO_2 surface are only weakly coupled, so the charge transport cannot be assumed adiabatic. Instead, a Landau-Zener-based description is appropriate for calculating hopping rates. This approach has been used successfully in similar oxide systems to account for cases where adiabatic treatment would overestimate charge transfer. For example, Wu and Ping [38] found that, in $BiVO_4$ small-polaron mobility, accounting for partial nonadiabaticity via Landau-Zener theory was essential; neglecting it led to qualitatively wrong mobility predictions.

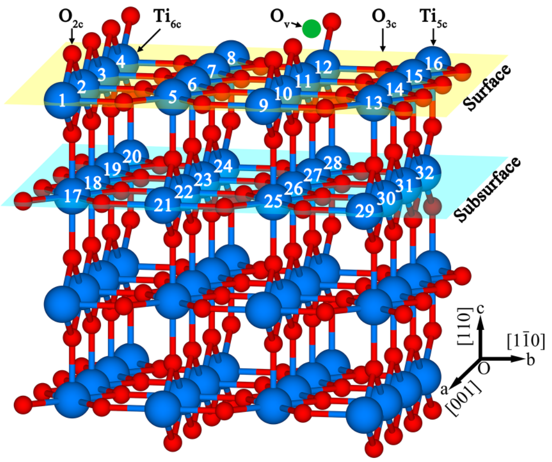

FIG. 1. A (4 × 2) rutile TiO_2 (110) surface with a bridge oxygen vacancy (O_v) at the surface. It should be noticed that the Ti atoms in the first two layers are distinguished by atom number, which can be denoted as Ti[*n*] for short. The Ti, O, and O_v are shown as blue, red, and green spheres, respectively.

Based on the above result, the polaron carrier mobility can be obtained from Einstein's relation as [39]

$$\mu = \frac{eD}{k_B T}, \tag{10}$$

where the symbol D is the diffusion coefficient, which can be calculated as [40,41]

$$D = R^2 n k_{et}, \tag{11}$$

where R is the polaron transfer distance from the initial site α to the final site β, and n is the number of polarons.

III. RESULTS AND DISCUSSIONS

A. Bipolarons spatial distribution on the reduced rutile TiO_2 (110) surface

A (4 × 2) supercell with four trilayers is chosen to model the rutile TiO_2 (110) surface as shown in Fig. 1. It contains fivefold-coordinated (Ti_{5c}) and sixfold-coordinated (Ti_{6c}) titanium atoms as well as twofold-coordinated (O_{2c}) and threefold-coordinated (O_{3c}) oxygen atoms at the surface. One bridge oxygen vacancy (O_v) is introduced at the surface, corresponding to a surface O_v concentration of $\frac{1}{8}$. Although an O_v is introduced to the rutile TiO_2 surface, the system remains in a neutral charge state. Generally, the introduction of one O_v simultaneously brings two excess electrons to the system, and it has been reported that these two excess electrons favor localization at Ti^{4+} atoms, forming small polarons in the reduced rutile TiO_2 [9,20,34,42,43].

To assess the stability of bipolarons, the possible spatial distribution of the two polarons is systematically studied, and the corresponding result is shown in Fig. 2, together with the detailed relative energy summarized in Table S1 in the Supplemental Material [44]. It should be noted that only equivalent Ti atoms are considered, and polarons in the first two trilayers are chosen. The resulting preferential sites for bipolaron localization are as follows: For the bipolarons at the surface (called the *surface state* in the following), the lowest E_{diff} is at

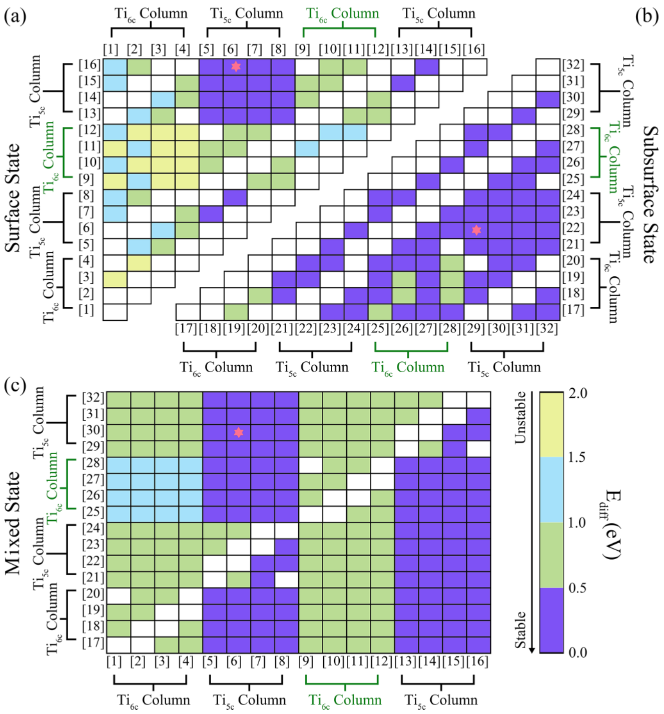

FIG. 2. Relative energy (E_{diff}) of the bipolaron occupation in different spatial locations. The two polarons of the bipolaron localized at (a) surface, (b) subsurface, and (c) separate surface and subsurface Ti atoms. The most stable location is marked by a pink star, and the green font indicates the Ti$_{6c}$ column where O$_{\mathrm{v}}$ is located.

~0.05 eV with the two polarons occupying sites at the Ti atoms around the O$_{\mathrm{v}}$. For the case of bipolarons at the subsurface (called the *subsurface state*), it has the lowest total energy, which can be set as a reference for convenience, and the corresponding occupied sites are at subsurface Ti [22] and Ti [29] atoms. Apart from the surface and subsurface bipolarons, the case of bipolarons consisting of one polaron at a surface Ti site and the other polaron at a subsurface Ti site (called the *mixed state* in the following) is also considered. The lowest E_{diff} is at ~0.01 eV, with the bipolarons occupying surface Ti [6] and subsurface Ti [30]. Furthermore, one of the bipolarons has a preference to occupy the Ti$_{5c}$ column, consistent with the result of Kowalski *et al.* [45]. The other bipolaron prefers to occupy subsurface Ti [22] and Ti [29] atoms, consistent with previous results of Shibuya *et al.* [10,11]. In all, it can be concluded that the most stable bipolaron configuration is at subsurface Ti [22] and Ti [29], with the second most stable configuration a mixed state of surface Ti [6] and subsurface Ti [30]. The third stable case is that of surface Ti [6] and Ti [16]. From the other side, it can be found that the bipolarons in Ti [22] and Ti [29] sites far from the O$_{\mathrm{v}}$ site (corresponding to O$_{\mathrm{v}}$ in +2) are ~0.62 eV lower than one polaron in Ti [11] and Ti [22] sites at O$_{\mathrm{v}}$ (corresponding to O$_{\mathrm{v}}$ in +1) as well as 1.36 eV lower than two polarons in Ti [11] and Ti [12] sites at O$_{\mathrm{v}}$. At the same time, the stability of the bipolarons was also checked by the HSE06 functional. Taking the two most stable configurations as an example, the HSE06 result shows the same tendency as that of our C-DFT+U result, as shown in Table S2 in the Supplemental Material [44], suggesting the reliability of our result. Furthermore, we also estimated the non-Koopmans deviation [46] (ΔE_{nk}) for the defect states of Ti^{3+} through fixed-charge calculation, as shown in Table S3 in the Supplemental Material [44]. The DFT+U calculation shows $\Delta E_{nk} = -0.39$ eV, which is much smaller than the expected $\Delta E_{nk} = -0.82$ eV with a semilocal GGA functional but close to the HSE06 result of $\Delta E_{nk} = -0.35$ eV. This confirms that our Hubbard-corrected functional yields nearly piecewise-linear total-energy behavior for the defect occupancy, effectively satisfying Koopmans's condition for the polaronic state.

To study the energetic contributions to the stability of bipolarons, the lattice distortion energy (E_{lat}) and electronic energy (E_{el}) are calculated. Both energies are components of the formation energy (E_{pol}) [47]. The corresponding result is summarized in Table S4 in the Supplemental Material [44]. Clearly, the bipolarons at subsurface Ti [22] and Ti [29] have the lowest E_{lat} of ~1.16, ~0.39, and 0.12 eV lower than the second and third cases, respectively. At the same time, the corresponding electronic energy (E_{el}) is ~−1.91 eV to stabilize this state. On the other hand, the dipole-dipole interaction perpendicular to the slab is also checked. Taking the three most stable configurations as an example, the calculations within dipole correction show E_{pol} at ~−0.03 eV (surface state), −0.80 eV (subsurface state), and −0.35 eV (mixed state), as shown in Table S4 in the Supplemental Material [44], which align with our original computational results of −0.15 eV (surface state), −0.75 eV (subsurface state), and −0.55 eV (mixed state), respectively. Therefore, the bipolarons at the subsurface have the lowest lattice distortion energy and the highest electron gain in energy, resulting in the most stable configuration.

Furthermore, the electronic density of states (DOS) is used to examine the stability of bipolarons localized in different sites. Taking the three most stable bipolarons as typical representations, the corresponding DOS is shown in Fig. 3. The valence band maximum consists of O 2p orbitals in all cases, and the conduction band minimum (CBM) consists mainly of Ti 3d orbitals, consistent with previously reported results [48]. The existence of bipolarons causes gap states below the CBM. For the most stable case (subsurface Ti [22] and Ti [29]), a pair of spin-symmetrical gap states appears at ~0.62 eV below the CBM. As for the second most stable case (surface Ti [6] and subsurface Ti [30]), two separated gap states appear at 0.62 and 0.97 eV below the CBM, respectively. In the third most stable case (surface Ti [6] and Ti [16]), a spin-symmetrical gap state appears ~0.90 eV below the CBM. Examining the band splitting of the Ti 3d orbitals in the three cases by crystal field theory combined with d-band center theory [49], a clear tendency can be found: For the bipolarons in the subsurface state, the splitting is largest (5.07 eV); in the mixed state, it is reduced (5.01 eV as shown in Table S5 in the Supplemental Material [44]); and the smallest splitting is found in the surface state (4.94 eV), showing a decreasing tendency, as shown in Fig. S2(a) in the Supplemental Material [44], together with the data in Table S5 in the Supplemental Material [44]. According to the crystal field theory, a larger splitting of the Ti 3d orbital means a more stable system. Although all the bipolarons are in the same crystal fields, the lattices are in different distortions, leading to different splittings of

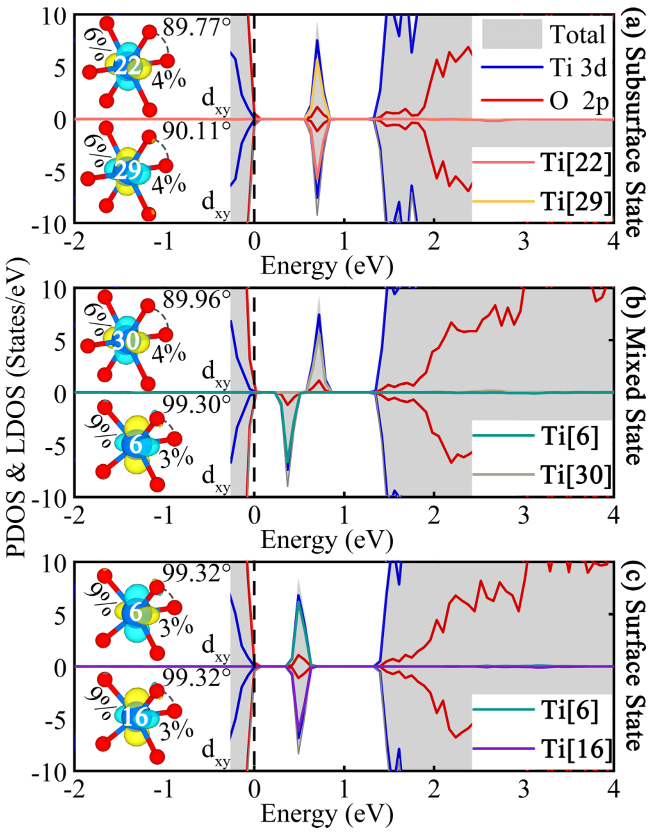

FIG. 3. Electronic density of states (DOS) for the bipolarons: (a) Surface state, (b) subsurface state, and (c) mixed state, corresponding to the three lowest relative energies.

the energy level. Furthermore, the calculated result is close to the crystal orbital Hamilton population result since it is also a weighted electronic DOS. Thus, bipolarons in the subsurface state (Ti [22] and Ti [29]) are the most stabilized from the electronic structure point of view.

Apart from *d*-orbital splitting, the orbital symmetry is also considered and shown in the inset of Fig. 3. Bipolarons favor occupancy of d_{xy} orbitals with a strong electrostatic repulsion from the ligand O atoms in the *x*-*y* plane. The stability can be sensitively influenced by the local structure. For the most stable bipolarons at subsurface Ti [22] and Ti [29] atoms, the Ti-O bond in the *x*-*y* plane is stretched by 6%, while the Ti-O bond in the *x*-*z* plane is only elongated by 4%. The case for the second most stable bipolarons in the mixed state at Ti [6] and Ti [16] is slightly different with the Ti-O bond elongation in *x*-*y* plane of ~7%. The polaron at the surface Ti [6] atom causes a Ti-O stretch by 9% in the *x*-*y* plane, which is ~0.09 Å larger than the Ti [22] atom in the above case, as shown in Fig. S2(b) in the Supplemental Material [44]. Therefore, bipolarons prefer to occupy the subsurface Ti atoms under both sides of the O_v site.

Apart from the orbital splitting and the symmetry, it is also interesting to understand the spatial distribution of bipolarons associated with the surface O_v. It has been reported by Zhao *et al.* [50] that the stability of bipolarons is strongly determined by the oxygen vacancy. Furthermore, Reticcioli *et al.* [9] found that the stability of bipolarons is a synergetic effect of repulsive interactions among the two polarons and the attractive interaction between the polarons and O_v. Thus, the electrostatic interaction between the polarons and O_v is further examined according to a point charge model, as shown in Fig. S1 in the Supplemental Material [44], which is strongly affected by the localized charges and their distance. It is well known that the longer the distance between the charges, the lower the repulsive $E_{\text{potential}}$. Here, we use S_{area} to denote the area of the triangle formed by the system of three point charges. Based on Eq. (2), the relationship of electrostatic potential energy ($E_{\text{potential}}$) and the area (S_{area}) involving bipolarons and O_v as well as the relative energies of the bipolarons is displayed in Fig. 4. The subsurface bipolarons (Ti [22] and Ti [29]) with the largest S_{area} exhibit the lowest $E_{\text{potential}}$, consistent with the lowest relative energy of bipolarons. These findings are like the result reported by Kowalski *et al.* [45]. Thus, bipolarons induced by O_v prefer subsurface sites around O_v due to the synergetic effect of repulsion and attraction among polarons and O_v.

B. Bipolarons transfer on the reduced rutile TiO_2 (110) surface

In addition to the spatial distribution, the transport behavior of bipolarons is also interesting since it is a key factor determining photoelectric efficiency. Here, combining C-DFT and Marcus theory, the transport properties of the three most stable bipolarons are systematically investigated along possible directions. The result is summarized in Table I, together with some detailed data in Fig. S3 in the Supplemental Material [44]. Like what is known for a perfect surface, a higher polaron transport rate is found along the [001] direction than along the [110] direction. The magnitude of the rate along the [001] direction can reach 2.42×10^{11} s^{-1}, which is ~5 orders larger than that along the [110] direction, consistent with previous results reported by Deskins *et al.* [31]. It is found that this larger transfer rate is strongly related to the smaller energy barrier along the [001] direction, where the energy barrier is ~0.17 eV lower than along the [110] direction. Therefore, bipolarons induced by surface O_v favor transfer along the [001] direction.

Apart from the [001] direction, polaron transfer from subsurface to surface along the [110] direction is also examined. Here, it should be mentioned that it is difficult to achieve stable polaron occupation at the surface Ti_{6c}, so the transmission of a polaron along the [110] direction to Ti_{6c} will not be common. The calculated results are displayed in Fig. 5(a) and the detailed data in Table S6 in the Supplemental Material [44]. The largest k_{et} occurs around the O_v site, with the largest value reaching 2.74×10^9 s^{-1} as the polaron transfer from Ti [27] to Ti [11] in an adiabatic process, which is ~2 orders higher than that of the perfect case. In the Ti_{5c} terminal case, the polaron transport from Ti [23] to Ti [7], the nonadiabatic transmission achieves a k_{et} value of 4.28×10^7 s^{-1}, quite close to the perfect case. For larger distances from O_v as in the case of transfer from Ti [22] to Ti [6] or Ti [5], a nonadiabatic transmission process can be found with a transfer rate k_{et} of only ~3.02×10^6 and 6.83×10^5 s^{-1}, respectively. Thus, the presence of the surface O_v can effectively influence the transport behavior of polarons around the vacancy. Particularly, compared with the regular surface Ti_{6c} case, the transfer rate

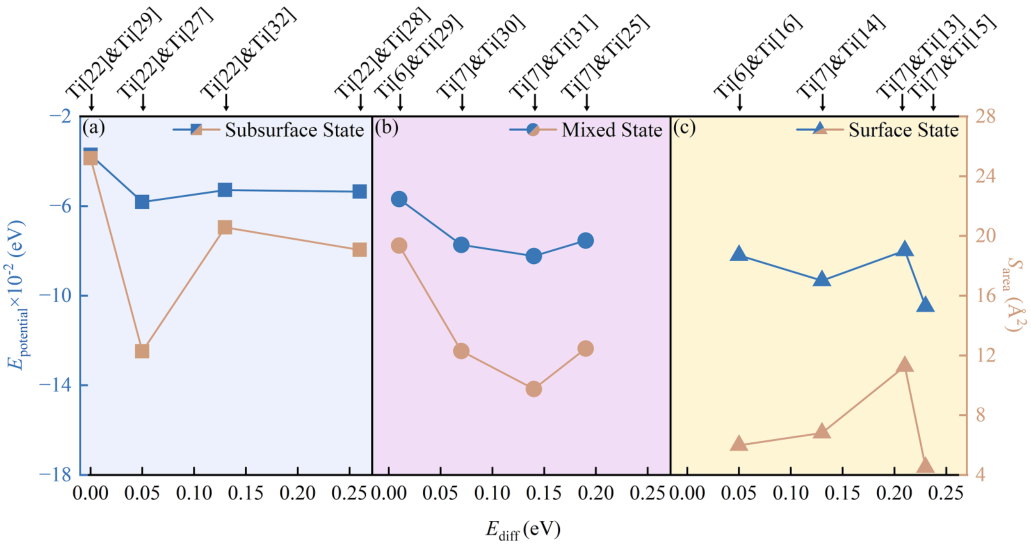

FIG. 4. Relationship of the electrostatic potential energy ($E_{\text{potential}}$) and the bipolaron area (S_{area}), plotted against the corresponding relative energies of the bipolarons. The corresponding bipolarions in (a) surface state, (b) subsurface state, and (c) mixed state, respectively.

can be 10^3 times larger for the case as the polaron transfers to the Ti_{6c} column involving O_v along the [110] direction. This phenomenon highlights the unique role of O_v. Further analysis suggests that this behavior may be closely related to local lattice distortions. The presence of O_v reduces the distance between Ti [27] and Ti [11], facilitating the leap of a polaron along the [110] direction with an energy barrier of only 0.25 eV. Additionally, a large electronic coupling strength (H_{ab}) of 55 meV between the two polaron states facilitates the transfer process, as shown in Fig. 5(b). This interesting result is in good agreement with the previous findings by Papageorgiou *et al.* [51], where a maximum response current exists around the O_v site in STM experiments. Therefore, our results effectively uncover the underlying mechanism of the strong response in STM experiments, which is related to the high polaron transport rate from subsurface to surface around a surface oxygen vacancy.

C. Water effect on polaron behavior on the reduced rutile TiO_2 (110) surface

In real devices, it is inevitable to deal with humid environments. Thus, understanding the effect of water molecules on the polaron properties is of great importance. Here, a water molecule adsorbed at reduced rutile TiO_2 (110) surfaces is initially considered, and the corresponding results are summarized in Table S7 in the Supplemental Material [44]. Compared with regular surface Ti_{5c} sites, water molecules have a stronger adsorption energy at O_v sites, with the adsorption energy of −1.74 eV (with the corresponding relative energy difference at ∼0.88 eV), as shown in Fig. S4 in the Supplemental Material [44]. The adsorbed water at an O_v site will spontaneously split into two hydroxyls OH, leading to the filling of the vacancy and leaving two neighboring bridging hydroxyl groups, consistent with previous experimental and theoretical results [52–55]. In this situation (see area I as denoted by $2O_bH$ in Fig. 6), the spatial distribution of the bipolarons is also evaluated, and the corresponding results are shown in Table S9 in the Supplemental Material [44]. Like the O_v case, the most stable bipolarons are located at subsurface states at Ti [22] and Ti [29] atoms. The second most stable bipolarons occur in the mixed state (surface Ti [6] and subsurface Ti [30] atoms) with the relative energy of ∼0.03 eV, together with the third most stable one in the surface state (Ti [6] and Ti [13] atoms), with a relative energy of ∼0.07 eV, consistent with the findings by Wang *et al.* [56].

Based on the described filling of the O_v site, different water coverages are further considered, and the typical model is shown in Fig. 6. For simplicity, water adsorbed at surface

TABLE I. Transport parameters of bipolarons transfer along possible directions on a reduced Rutile TiO_2 (110) surface. The given parameters are reorganization energy (λ), electron coupling strength ($H_{\alpha\beta}$), transfer probability (κ), nearest Ti-Ti distance ($d_{\text{Ti-Ti}}$), mobility of carrier polaron (μ), and the diffusion coefficient (D).

Model	Direction	λ (eV)	$H_{\alpha\beta}$ (meV)	κ	Transfer mode	ΔG^* (eV)	k_{et} (s^{-1})	$d_{\text{Ti-Ti}}$ (Å)	D (cm^2/s)	μ(cm^2/V s)
Like-bulk clusters [31]	[111]	1.23	10	0.02	Nonadiabatic	0.31	3.66×10^6	3.61	1.91×10^{-8}	7.42×10^{-7}
	[001]	1.15	200	1.00	Adiabatic	0.09	7.65×10^{11}	2.97	1.35×10^{-3}	5.24×10^{-2}
Perfect slab [24]	[110]	1.28	12	0.08	Nonadiabatic	0.31	1.42×10^7	3.55	1.07×10^{-7}	4.13×10^{-6}
	[001]	1.07	101	0.98	Adiabatic	0.18	1.80×10^{11}	2.96	9.44×10^{-4}	3.65×10^{-2}
O_v	[110]	1.29	6	0.03	Nonadiabatic	0.32	3.02×10^6	3.55	2.28×10^{-8}	8.82×10^{-7}
	[001]	0.87	71	0.91	Adiabatic	0.15	2.42×10^{11}	2.99	1.29×10^{-3}	5.00×10^{-2}

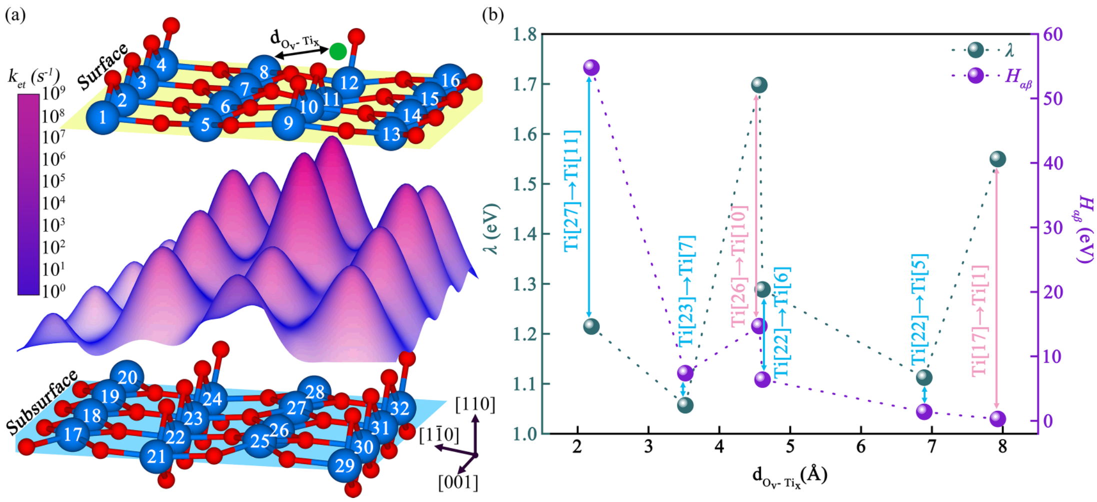

FIG. 5. (a) Transfer rate (k_{et}) of bipolaron transport from subsurface to surface along the [110] direction. (b) Change of the transport parameters (λ and $H_{\alpha\beta}$) with the increasing distance between O_v and the surface Ti atom where the polaron is transferred to. The arrows in blue and pink indicate the polaron transported to surface Ti_{5c} and Ti_{6c}, respectively.

Ti_{5c} represents the water coverage of $\frac{1}{8}$ monolayer, which can be denoted as $2O_bH + \frac{1}{8}$ for short. Considering the hydrogen bonding effect from the bridge OH as reported by Fischer *et al.* [22], the placement of the water can form two binding modes, as depicted in area II of Fig. 6. The calculations show that the water positioned in the $H_{water} - O_{bridge}$ state is ~0.14 eV lower than that in the H_{water}-$O_{bridge}H$ state, showing that the H_{water}-O_{bridge} state is more stable, as shown in Table S8 in the Supplemental Material [44]. In the most stable water adsorption case, the bipolarons favor localization at surface Ti [6] and Ti [13]. Furthermore, the dissociation of the water molecule at $\delta = 2O_bH + \frac{1}{8}$ (area III of Fig. 6) is also considered, as in the work of Chen *et al.* [57], it was discovered that bipolarons have a dual-functional role both as inhibitor and promotor of a surface water dissociation. Our calculations show that the intact water molecule is more stable than the dissociated one, as seen in Table S8 in the Supplemental Material [44], consistent with previous calculations. Therefore, the localization of the bipolarons can be altered at low water concentration.

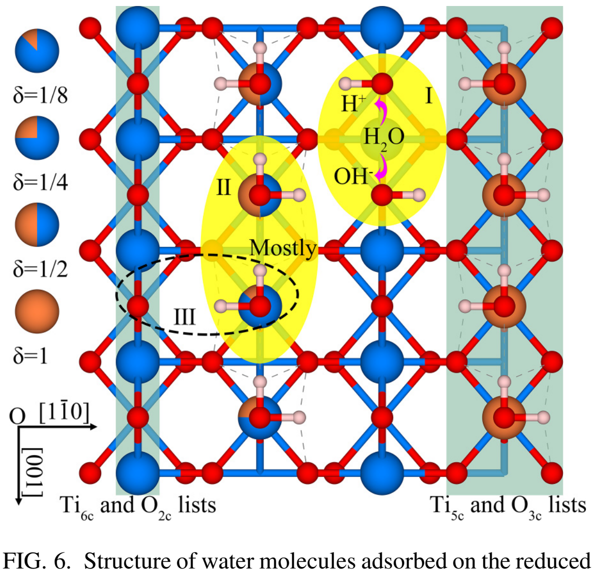

FIG. 6. Structure of water molecules adsorbed on the reduced rutile (110) surface in different coverages. The coverage rate is denoted by the brown color in the Ti spheres. The Ti, O, and H atoms are blue, red, and pink spheres, respectively.

With the increasing water coverage, the spatial distribution of the bipolarons is further considered, and the calculated result is shown in Fig. 7(a), together with the detailed data in Table S9 in the Supplemental Material [44]. Relative to the $2O_bH + \frac{1}{8}$ case, the most stable state of the bipolarons still appears in the surface state until a water concentration ratio of one. Looking at the variation between each state, the E_{diff} of bipolarons in the subsurface and mixed state is gradually increasing with the water concentration, reaching a maximum value of 0.24 eV for the subsurface state when the ratio reaches $2O_bH + 1$. Thus, the increase of the water coverage will extract the bipolarons from the inner site to a surface site, facilitating surface photoelectric reactions.

Apart from the stability, we also study the transport behavior of bipolarons under different water coverages. It is worth noting that subsurface Ti [22] is chosen as the initial site since the bipolarons in this site are most stable among the subsurface and mixed states regardless of dry or water dissociative adsorption conditions. The water coverage has little effect on the polaron transfer rate along the [1$\bar{1}$0] and [$\bar{1}\bar{1}$0] directions (Fig. S5 in the Supplemental Material [44]), consistent with previous studies [24]. We therefore focused on the bipolaron transfer along the [110] and [001] directions. The corresponding results are shown in Fig. 7(b), together with the detailed data in Table S10 in the Supplemental Material [44]. Unexpectedly, the transfer of the bipolarons can be significantly affected by the water coverage along both directions. Taking the [001] direction as an example, the transfer rate of the bipolarons reaches a maximum value of 8.40×10^{12} s^{-1} at $2O_bH + \frac{1}{2}$. Thus, this transport direction should be the primary one as $\delta \leqslant 2O_bH + \frac{1}{4}$ since the transfer rate along [001] is much larger than that along the [110] direction. However, as $\delta \geqslant 2O_bH + \frac{1}{2}$, the transport rate of the bipolarons along the [110] direction increases sharply, reaching the value

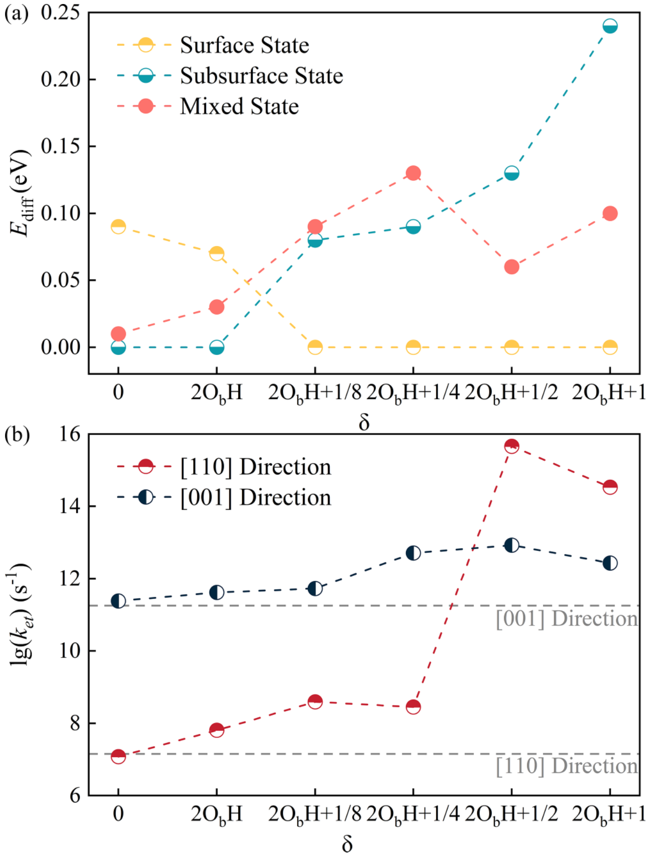

FIG. 7. (a) Relative energy (E_{diff}) of bipolarons for different surface water coverages. (b) Transport behavior of bipolarons along typical directions for different water coverages, together with the dry surface for comparison. The lg(k_{et}) denotes the $\log_{10}(k_{et})$ for short.

of 4.57×10^{15} s^{-1}, even larger than that of the [001] direction, showing the potential of bipolaron transfer from the inner site. Although the transfer rate shows a slight decrease, it is still much higher than that along the [001] direction as the water concentration at $2O_bH + 1$. Therefore, the coverage of water molecules can effectively influence the spatial distribution and transport behavior of bipolarons at the reduced rutile TiO_2 (110) surface.

To understand the underlying mechanism of the influence of the water coverage on bipolarons transport, we examine the transport parameters such as λ, $H_{\alpha\beta}$, and ΔG^*. The corresponding results are depicted in Fig. 8. The parameter λ shows almost no change with the increasing water coverage along both directions. However, the case for the other two parameters is quite different. Along the [001] direction, the fluctuations of $H_{\alpha\beta}$ and ΔG^* are extremely small (~0.1 eV). As for the [110] direction, when $\delta \leqslant 2O_bH + \frac{1}{4}$, the variation of $H_{\alpha\beta}$ is still relatively small in the range of 30 meV, together with a high ΔG^* of ~0.3 eV, indicating a nonadiabatic transport process. However, as δ increases to $2O_bH + \frac{1}{2}$, a pronounced trend reversal in $H_{\alpha\beta}$ and ΔG^* can be seen. For the [110] direction, the value of $H_{\alpha\beta}$ can reach up to 472 meV, together with a small ΔG^* barrier, indicating an adiabatic transport process. Therefore, the electronic coupling between initial and final states is identified as the primary determining factor for the calculated transport characteristics.

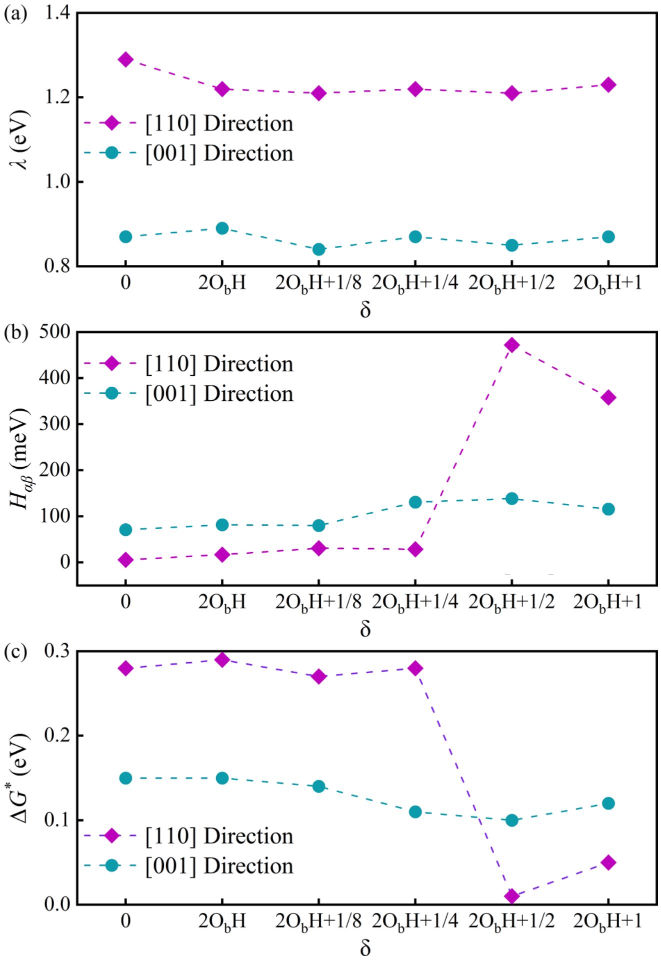

FIG. 8. Change of the transport parameters of bipolarons as a function of water coverage δ and the corresponding transport parameters: (a) Reorganization energy (λ), (b) electron coupling strength ($H_{\alpha\beta}$), and (c) transition barrier (ΔG^*).

IV. CONCLUSIONS

In summary, we explored the spatial distribution and transport properties of bipolarons induced by oxygen vacancies on reduced rutile TiO_2 (110) surfaces using C-DFT. Our results demonstrate that bipolarons energetically prefer subsurface sites, followed by a mixed surface-subsurface configuration, while a geometry involving only surface sites in the vicinity of the O_v is the least energetically favored localization. This unique behavior can be attributed to factors such as the electronic Ti 3*d* orbital splitting, the orbital symmetry, and the electrostatic potential obtained from a simple point charge model. Notably, the polaron transfer rate gradually decreases as a function of the distance from O_v along the [110] direction. The introduction of water can strongly change the spatial distribution of bipolarons, as in the presence of water, they alternate their preferred localization sites from subsurface to surface. Also, the bipolaron transport characteristics depend on the water coverage. As the water coverage is more than one-half monolayer, the preferred transfer direction of the polaron changes from the [001] direction to the [110] direction, i.e., toward the transport in the surface. This behavior is closely related to the variation of the electronic coupling strength and the energy barrier under different water coverages. Our findings shed light on the distribution and transport properties of bipolarons as well as the influence of water on the reduced rutile TiO_2 (110) surface, providing valuable insights into the role of polarons in photoelectric applications.

ACKNOWLEDGMENTS

This work was supported by the National Natural Science Foundation of China (Grants No. 51572016, No. U1530401, No. 11704116, No. 11804090, No. 51472209, No. 11774298, No. U1401241, and No. 21503012), the project of the Hunan Provincial Department of Education (Grant No. 21B0485), and the Natural Science Foundation of Hunan Province, China (Grant No. 2023JJ30226). We thank the fund under the China Scholarship Council (Grants No. 202104890004 and No. 202208430047). We also acknowledge Dr. Rutong Si for valuable expertise and discussion.

DATA AVAILABILITY

The data supporting this study's findings are available within the article.

---

[1] A. Fujishima and K. Honda, Electrochemical photolysis of water at a semiconductor electrode, Nature (London) **238**, 37 (1972).

[2] P. Deák, B. Aradi, and T. Frauenheim, Oxygen deficiency in TiO_2: Similarities and differences between the Ti self-interstitial and the O vacancy in bulk rutile and anatase, Phys. Rev. B **92**, 045204 (2015).

[3] A. Janotti, J. B. Varley, P. Rinke, N. Umezawa, G. Kresse, and C. G. Van de Walle, Hybrid functional studies of the oxygen vacancy in TiO_2, Phys. Rev. B **81**, 085212 (2010).

[4] L. Liu and Y. Li, Understanding the reaction mechanism of photocatalytic reduction of CO_2 with H_2O on TiO_2-based photocatalysts: A review, Aerosol Air Qual. Res. **14**, 453 (2014).

[5] W.-J. Yin, B. Wen, C. Zhou, A. Selloni, and L.-M. Liu, Excess electrons in reduced rutile and anatase TiO_2, Surf. Sci. Rep. **73**, 58 (2018).

[6] F. Cheng, L. Liang, G. Lin, and S. Xi, Enhanced photoelectrocatalysis in porous single crystalline rutile titanium dioxide electrodes, J. Mater. Chem. A **12**, 3879 (2024).

[7] C. Wu, Z. Gao, S. Gao, Q. Wang, H. Xu, Z. Wang, B. Huang, and Y. Dai, Ti^{3+} self-doped TiO_2 photoelectrodes for photoelectrochemical water splitting and photoelectrocatalytic pollutant degradation, J. Energy Chem. **25**, 726 (2016).

[8] H. Liang, M. Yu, Y. Sun, J. Lu, and J. Niu, Unraveling the reinforced photoelectrocatalytic activity and stability via unique configuration of P^{3+}-O_v-Ti^{3+} in TiO_{2-x} nanotube array, Chem. Eng. J. **435**, 134908 (2022).

[9] M. Reticcioli, M. Setvin, M. Schmid, U. Diebold, and C. Franchini, Formation and dynamics of small polarons on the rutile TiO_2 (110) surface, Phys. Rev. B **98**, 045306 (2018).

[10] T. Shibuya, K. Yasuoka, S. Mirbt, and B. Sanyal, Bipolaron formation induced by oxygen vacancy at rutile TiO_2(110) surfaces, J. Phys. Chem. C **118**, 9429 (2014).

[11] T. Shibuya, K. Yasuoka, S. Mirbt, and B. Sanyal, Subsurface polaron concentration as a factor in the chemistry of reduced TiO_2 (110) Surfaces, J. Phys. Chem. C **121**, 11325 (2017).

[12] N. A. Deskins, R. Rousseau, and M. Dupuis, Distribution of Ti^{3+} surface sites in reduced TiO_2, J. Phys. Chem. C **115**, 7562 (2011).

[13] C. Di Valentin, G. Pacchioni, and A. Selloni, Electronic structure of defect states in hydroxylated and reduced rutile TiO_2 (110) surfaces, Phys. Rev. Lett. **97**, 166803 (2006).

[14] C. J. Calzado, N. C. Hernández, and J. F. Sanz, Effect of on-site Coulomb repulsion term U on the band-gap states of the reduced rutile (110) TiO_2 surface, Phys. Rev. B **77**, 045118 (2008).

[15] S. Falletta and A. Pasquarello, Polaron hopping through piecewise-linear functionals, Phys. Rev. B **107**, 205125 (2023).

[16] S. McBride, W. Chen, T. Cuk, and G. Hautier, Do small hole polarons form in bulk Rutile TiO_2? J. Phys. Chem. Lett. **16**, 2333 (2025).

[17] J. Li, T. Wang, S. Xia, W. Chen, Z. Ren, M. Sun, L. Che, X. Yang, and C. Zhou, Site-selective excitation of Ti^{3+} ions in rutile TiO_2 via anisotropic intra-atomic $3d \rightarrow 3d$ transition, JACS Au **4**, 491 (2024).

[18] Z. Wang *et al.*, Localized excitation of Ti^{3+} ions in the photoabsorption and photocatalytic activity of reduced Rutile TiO_2, J. Am. Chem. Soc. **137**, 9146 (2015).

[19] L. Yan, J. E. Elenewski, W. Jiang, and H. Chen, Computational modeling of self-trapped electrons in Rutile TiO_2, Phys. Chem. Chem. Phys. **17**, 29949 (2015).

[20] A. Janotti, C. Franchini, J. Varley, G. Kresse, and C. Van de Walle, Dual behavior of excess electrons in Rutile TiO_2, Phys. Status Solidi RRL **7**, 199 (2013).

[21] K. Morita, M. J. Golomb, M. Rivera, and A. Walsh, Models of polaron transport in inorganic and hybrid organic-inorganic titanium oxides, Chem. Mater. J. **35**, 3652 (2023).

[22] S. A. Fischer, W. R. Duncan, and O. V. Prezhdo, *Ab initio* nonadiabatic molecular dynamics of wet-electrons on the TiO_2 surface, J. Am. Chem. Soc. **131**, 15483 (2009).

[23] C. Gao, L. Zhang, Q. Zheng, and J. Zhao, Tuning the lifetime of photoexcited small polarons on rutile TiO_2 surface via molecular adsorption, J. Phys. Chem. C **125**, 27275 (2021).

[24] Y.-B. Li, R. Si, B. Wen, X.-L. Wei, N. Seriani, W.-J. Yin, and R. Gebauer, The role of water molecules on polaron behavior at rutile (110) surface: A constrained density functional theory study, J. Phys. Chem. Lett. **15**, 1019 (2024).

[25] J. VandeVondele, M. Krack, F. Mohamed, M. Parrinello, T. Chassaing, and J. Hutter, QUICKSTEP: Fast and accurate density functional calculations using a mixed Gaussian and plane waves approach, Comput. Phys. Commun. **167**, 103 (2005).

[26] J. Heyd, G. E. Scuseria, and M. Ernzerhof, Hybrid functionals based on a screened Coulomb potential, J. Chem. Phys. **118**, 8207 (2003).

[27] W.-J. Yin, M. Krack, B. Wen, S.-Y. Ma, and L.-M. Liu, CO_2 capture and conversion on rutile TiO_2 (110) in the water environment: Insight by first-principles calculations, J. Phys. Chem. Lett. **6**, 2538 (2015).

[28] Z. Chai, R. Si, M. Chen, G. Teobaldi, D. D. O. Regan, and L.-M. Liu, Minimum tracking linear response Hubbard and Hund corrected density functional theory in CP2K, J. Chem. Theory Comput. **20**, 8984 (2024).

[29] S. Grimme, J. Antony, S. Ehrlich, and H. Krieg, A consistent and accurate *ab initio* parametrization of density functional dispersion correction (DFT-D) for the 94 elements H-Pu, J. Chem. Phys. **132**, 154104 (2010).

[30] P. Oruç, N. Turan, S. Cavdar, N. Tuğluoğlu, and H. Koralay, Investigation of dielectric properties of amorphous, anatase, and rutile TiO_2 structures, J. Mater. Sci. Mater. Electron. **34**, 498 (2023).

[31] N. A. Deskins and M. Dupuis, Electron transport via polaron hopping in bulk TiO_2: A density functional theory characterization, Phys. Rev. B **75**, 195212 (2007).

[32] B. S. Brunschwig, J. Logan, M. D. Newton, and N. Sutin, A semiclassical treatment of electron-exchange reactions. Application to the hexaaquoiron (II)-hexaaquoiron (III) system, J. Am. Chem. Soc. **102**, 5798 (1980).

[33] C. Zener, Non-adiabatic crossing of energy levels, Proc. R. Soc. Lond. A **137**, 696 (1932).

[34] C. Zener, Dissociation of excited diatomic molecules by external perturbations, Proc. R. Soc. Lond. A **140**, 660 (1933).

[35] S. P. Porto, P. A. Fleury, and T. C. Damen, Raman spectra of Ti, Mg, Zn, Fe, and Mn, Phys. Rev. **154**, 522 (1967).

[36] R. A. Marcus and N. Sutin, Electron transfers in chemistry and biology, Biochim. Biophys. Acta, Rev. Bioenerg. **811**, 265 (1985).

[37] P. K. Behara and M. Dupuis, Electron transfer in extended systems: Characterization by periodic density functional theory including the electronic coupling, Phys. Chem. Chem. Phys. **22**, 10609 (2020).

[38] F. Wu and Y. Ping, Combining Landau-Zener theory and kinetic Monte Carlo sampling for small polaron mobility of doped $BiVO_4$ from first-principles, J. Mater. Chem. A **6**, 20025 (2018).

[39] A. Einstein, *Investigations on the Theory of the Brownian Movement* (Dover Publications, Inc., Mineola, 1956).

[40] R. R. Heikes and W. D. Johnston, Mechanism of conduction in Li-substituted transition metal oxides, J. Chem. Phys. **26**, 582 (1957).

[41] J. B. Goodenough, Metallic oxides, Prog. Solid State Chem. **5**, 145 (1971).

[42] S. Livraghi, M. Rolando, S. Maurelli, M. Chiesa, M. C. Paganini, and E. Giamello, Nature of reduced states in titanium dioxide as monitored by electron paramagnetic resonance. II: Rutile and brookite cases, J. Phys. Chem. C **118**, 22141 (2014).

[43] G. Kolesov, B. A. Kolesov, and E. Kaxiras, Polaron-induced phonon localization and stiffening in rutile TiO_2, Phys. Rev. B **96**, 195165 (2017).

[44] See Supplemental Material at http://link.aps.org/supplemental/10.1103/ckws-yk2c for additional information about the C-DFT method and discussion of the related simulation results. The Supplemental Material also contains Refs. [24,46,47].

[45] P. M. Kowalski, M. F. Camellone, N. N. Nair, B. Meyer, and D. Marx, Charge localization dynamics induced by oxygen vacancies on the TiO_2 (110) surface, Phys. Rev. Lett. **105**, 146405 (2010).

[46] I. Dabo, M. Cococcioni, and N. Marzari, Non-Koopmans corrections in density-functional theory: Self-interaction revisited, arXiv:0901.2637.

[47] M. Setvin, C. Franchini, X. Hao, M. Schmid, A. Janotti, M. Kaltak, C. G. Van de Walle, G. Kresse, and U. Diebold, Direct view at excess electrons in TiO_2 Rutile and anatase, Phys. Rev. Lett. **113**, 086402 (2014).

[48] D. O. Scanlon, C. W. Dunnill, J. Buckeridge, S. A. Shevlin, A. J. Logsdail, S. M. Woodley, C. R. A. Catlow, M. J. Powell, R. G. Palgrave, and I. P. Parkin, Band alignment of rutile and anatase TiO_2, Nat. Mater. **12**, 798 (2013).

[49] F. Ando, T. Gunji, T. Tanabe, I. Fukano, H. D. Abruna, J. Wu, T. Ohsaka, and F. Matsumoto, Enhancement of the oxygen reduction reaction activity of Pt by tuning its d-band center via transition metal oxide support interactions, ACS Catalysis **11**, 9317 (2021).

[50] L. Zhao, B. Magyari-Köpe, and Y. Nishi, Polaronic interactions between oxygen vacancies in rutile TiO_2, Phys. Rev. B **95**, 054104 (2017).

[51] A. C. Papageorgiou, N. S. Beglitis, C. L. Pang, G. Teobaldi, G. Cabailh, Q. Chen, A. J. Fisher, W. A. Hofer, and G. Thornton, Electron traps and their effect on the surface chemistry of TiO_2 (110), Proc. Natl. Acad. Sci. USA **107**, 2391 (2010).

[52] I. M. Brookes, C. A. Muryn, and G. Thornton, Imaging water dissociation on TiO_2 (110), Phys. Rev. Lett. **87**, 266103 (2001).

[53] Q. Guo, C. Zhou, Z. Ma, and X. Yang, Fundamentals of TiO_2 photocatalysis: Concepts, mechanisms, and challenges, Adv. Mater. **31**, 1901997 (2019).

[54] Q. Guo, Z. Ma, C. Zhou, Z. Ren, and X. Yang, Single molecule photocatalysis on TiO_2 surfaces: Focus review, Chem. Rev. **119**, 11020 (2019).

[55] Z. Zhang, K. Cao, and J. T. Yates, Defect-electron spreading on the TiO_2(110) semiconductor surface by water adsorption, J. Phys. Chem. Lett. **4**, 674 (2013).

[56] R. Wang and H. Fan, The location of excess electrons on H_2O/TiO_2 (110) surface and its role in the surface reactions, Mol. Phys. **116**, 171 (2018).

[57] J. Chen, C. Penschke, A. Alavi, and A. Michaelides, Small polarons and the Janus nature of TiO_2 (110), Phys. Rev. B **101**, 115402 (2020).